Theoretical description and experimental characterization of water content distributions in hydrogen PEM fuel cells.

C.F. Zinola *

Electrochemical Engineering Group, Universidad de la República, J.E. Rodó 1843, C.P. 11100, Montevideo, Uruguay.

**corresponding author, fzinola@fcien.edu.uy*

Abstract

An analytical solution of water mass balance equation was obtained considering diffusion and electroosmotic drag fluxes under non steady state regimes. The theoretical predicted profiles in a *membrane electrode assembly* were compared experimentally in a single polymer electrolyte hydrogen/oxygen fuel cell changing operating conditions such as, flow velocity, current density and temperature. The specific anodic and cathodic areas were calculated using the carbon monoxide anodic *stripping* method (ca. 17000 cm^2). The electroosmotic drag coefficient was determined with electrochemical isopiestic methods showing temperature invariance, *i.e.* 2.3 between 313 and 353 K for water contents less than 5, but when reaching 20 it increased to 3.2.

Polarization curves were attained galvanodynamically in a single fuel cell showing a strong dependence on water residence (performing with distinct water amounts and conditions). Internal resistance (0.59 to 0.24 Ω cm^{-2}) and open circuit potentials (0.90 to 0.38 V) were affected by water reduction (from 0.8 to 0.4 units). Continuous water recycling of the fuel cell was adopted to preserve the shape and characteristic parameters of the fuel cell under full operation with excellent results.

***Keywords*;** water content, electroosmotic drag, hydrogen, fuel cell.

Introduction

Proton exchange membrane fuel cells (PEMFCs) are capable electrochemical devices for energy-conversion for transport and stationary uses. The preparing of an optimum electrocatalyst membrane composite seems to be the heart of the device, however other important keys need to be solved, *i.e.* decrease in the cathodic overpotential and constant humidification of the membrane [1, 2]. In this sense, the assimilation of PEMFCs to industrial applications [2] depends on the success of using a proper ionomeric polymer electrolyte membrane since they exhibit excellent proton conductivities only in the wet state.

Water balance has been proven to be critical not only for the performance but also for the durability of PEMFCs. The water cycle within the porous membrane and catalyst layers is controlled by electroosmotic drag flow, back diffusion, capillary effects and pressure driven hydraulic permeation (when a pressure gradient is used). Since there are at least 3 factors that have to be kept for a proper water balance, lack or excess of water is a critical point to reach in a balanced way. Since many years ago, authors tried new humidification methods. Reid [3] moistens a reactant by passing it through a heated water tank, while Nguyen and White [4] proposed a direct water spray into the gas stream. Chow and Wozniczka [5] developed a membrane humidifier skilled of attending water vapour to a reactant. Various internal and external hydration methods of polymer electrolyte membranes cover physical and chemical methods while the second detailed gas bubbling, direct injection, humidifier devices, etc. [6]

Moreover, deliquescent materials (calcium chloride/bromide and potassium phosphate di acid/acetate) absorb and retain constant amounts of water to keep a certain and known membrane proton conductivity even at high temperatures [7].

In the present work various methods were assayed; anodic injection of water, permanent external hydration of the membrane, cathodic recycling, etc, all of them were adjusted by the operation temperature, air flow rate, purge intervals, inlet gas water per cent and gas inlet pressure. One thinkable way to keep it impregnated is the water recycled to humidify the feed gases and then, water balance in the cell would be achieved without external humidification [8]. This simplified design is preferred for fuel cell applications since this recycled water can easily be measured and modelled.

The interaction between the thermal and water organization sometimes produces a significant temperature gradient across the membrane during fuel cell operation. However, this fact is not considered here since a single isothermal PEMFC will be employed with identical temperature-controlled bipolar plates that eliminates internal gradients. If the operation cell temperature lies below 68^{o}C and there is no pressure gradient between anode and cathode, the hydraulic permeation is negligible compared to back diffusion and electroosmotic drag [9, 10]. Back diffusion increases with water contents and almost in one order of magnitude between 2 and 22. In any way, the modelling of the water content as a function of water vapour pressure, current density and proton conductivity is here envisaged with previous well proved equations.

Bernardi [11] was the first to treat water balances through gas diffusion electrodes in PEMFCs. Besides, the pioneer work of Fuller and Newman [12] advanced theoretical derivations and isopiestic methods for the estimation of water/proton electroosmotic drags. Springer *et al*. [13] provided a comprehensive discussion to a complete PEMFC model under steady-state regimes. Nguyen and White treated a 2 D heat and mass transfer model for PEMFCs [4]. However, some of these were too

complicated and only numerical calculations were possible. Nevertheless, Okada *et al.* [14] obtained an exact analytical solution for a 1 D water transport equation either with semi-infinite or with finite boundary conditions. On the other hand, a 1 D analytical model was envisaged by Park and Oh [15] to examine the moistening capacity of a Nafion membrane humidifier. The humidity and permeability of a Nafion membrane was calculated as a function of membrane thickness. However, the relative humidity of the gas stream passed through the Nafion membrane humidifier was numerically modelled changing the gas flow rates [16] for the device geometric characteristics. Thus, Lee *et al.* [17] investigated the effect of temperature, pressure and diffusional layer thickness on the performance of a PEMFC using an iridium oxide anode and platinum cathode. They have found that the anodic entrance of water is the controlling diffusional process and that at high pressures the diffusion layer thickness has negligible effects on PEMFC responses.

The introduction of *AC* impedance technique helps to find a connection between water content and membrane resistance in large surface area PEMFC [16]. Karnik [18] dealt with the problem of water transport in a whole stack of PEMFCs, considering a difference between the water dragging and diffusion fluxes, being proportional to the number of cells expending fluxes relations of Springer *et al.* [13]. A 0-D isothermal model was introduced to predict the flooding and drying conditions in both electrodes at various current intensities. Anode water removal and cathode inlet humidification were specified on water balance requirements and maximum membrane water passage.

The effect of water content on the electrochemical properties of Nafion membranes was also envisaged using cyclic voltammetries and high frequency

resistances [19]. The specific real area was found to decrease with the diminution of the water content with a critical point founding reversal water electrolysis and carbon corrosion. A 1 D analytical model developed for a 50 cm^2 PEMFC with five-channel serpentine flow field was reported [20]. Cell voltage, water content within the membrane and gas diffusion layers were experimentally measured by neutron radiography. The results showed a good agreement for a comprehensive set of different operating conditions of the cell considering all type of overpotentials including the ohmic decreases by catalyst coatings, bipolar plates, membranes, gas diffusion layers, etc.

Many attempts have been made using 2D and 3D models to solve the governing equations empirically or numerically using computation programs. One of the authors encouraging analytical solutions for the next up between fundamental electrochemical processes and engineering of PEMFCs was Kulikovsky with many papers condensed in [21]. He gave a 1 D and 2 D exact analytical description by modelling the catalyst layer performance with good description of the electrochemical behaviour to thermal stability. However, the characteristics of membrane water content and stability were not developed as well.

On the other hand, cooling plates at 2 phase models accounting for the mass, momentum, energy and charge conservations has been design using a phenomenological view for the membrane and an agglomerate catalytic layer. However, the equations were solved numerically to predict the number of optimal plates to keep the membrane well hydrated [22]. A 3D Lattice Boltzmann simulation method [23] was also employed to study pore-scale fluid flow and mass transfer in asymmetric membranes. A composite of 3 layers was considered; sponge-like porous-

finger-like hole- skin layer. The effect of annealing and permeability of the porous support was considered with mass transport equations. In spite of changing the composite membrane, water diffusion was enhanced after dipping the skin layer thickness. To avoid large computational times for numerical solutions in PEMFCs a novel method was employed reducing the time two orders of magnitude using average properties in 3D counterparts [24]. This provided important information for PEM cell/stack design without interminable computations iterations. The validation was conducted with Monte Carlo simulations at a single cell and stack levels.

In this work, an attempt is made to solve analytically the problem of the water content considering diffusion and electroosmosis fluxes as a function of membrane thickness and time. The water electroosmotic drag coefficient was determined by an electrochemical isopiestic cell and the real surface area of both electrodes was calculated by carbon monoxide anodic stripping voltammetry. The water recycling was employed as the method to keep the membrane properly humidified demonstrated through the PEMFC operation curves.

Theoretical considerations.

The resolution of differential equations associated with water and proton mass balances can be encouraged at laminar flows (more properly fully developed) under steady and non-steady isothermal regimes. The mixture of species is governed by Stefan-Maxwell interdiffusion as ideal components, but since the membrane is impermeable to the gaseous products, only protons with water are considered.

The source of water molar flux (mol cm^{-2} s^{-1}) has a true origin at the cathode side of the cell, $J_{H2O.}$ It is also related to the cell current density, j_{cell}, (A cm^{-2}) by the Faraday´s Law. Thus,

$$J_{H_2O} = j_{cell} / 2F \quad (1)$$

Being F the Faraday´s constant. In the membrane the water molar flux $J^{mem}_{H_2O}$ is connected to the anode $J^{an}_{H_2O}$ and cathode $J^{cat}_{H_2O}$ as;

$$J^{an}_{H_2O} = J^{mem}_{H_2O} \qquad J^{cat}_{H_2O} = j_{cell} / 2F + J^{mem}_{H_2O} \quad (2, 3)$$

Since diffusion occurs between and inside the pores, an effective diffusion coefficient applies through the membrane, which is able to model the transit when a proper geometry (cylindrical or conical) and porosity for ensembles is considered [14, 25, 26]. The amount of membrane water is defined by correcting the above molar fluxes by the electroosmotic drag flux $J^{osmo}_{H_2O}$ (from the catholyte to the anolyte shown in the scheme of Figure 1). Thus, it will be a certain dimensionless fraction of the current density according to [12, 14];

$$J^{osmo}_{H_2O} = \psi^{o}_{H_2O} j_{cell} / F \quad (4)$$

Being $\psi^{o}_{H_2O}$ the water electroosmotic dragging coefficient in the membrane or also known as transference number.

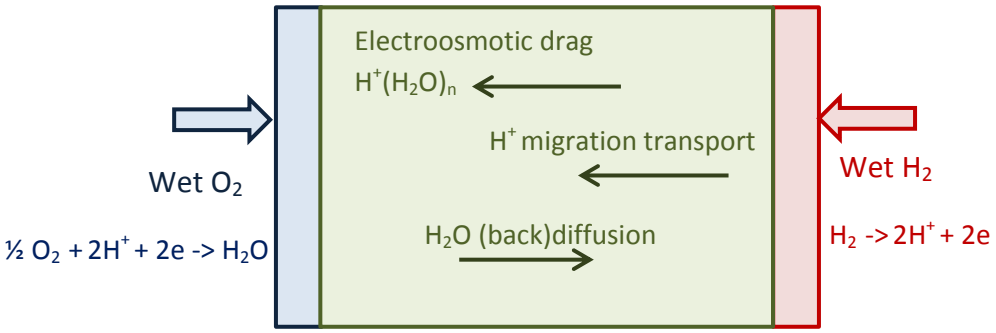

Figure 1.- Schematic diagram of the proton and water mass transfers, unidirectional modes, within the membrane of the PEMFC.

Thus, the water mass transference equation is then;

$$J_{H_2O} = J^{dif}_{H_2O} + J^{osmo}_{H_2O} = -D_{H_2O}\nabla C_{H_2O} + \psi^{o}{}_{H_2O}\, j_{cell} / F \qquad (5)$$

With the water diffusion molar flux as $J^{dif}_{H_2O}$, the water diffusivity as D_{H_2O} and the water gradient concentration vector as ∇C_{H_2O}.

Since we take the estimation of a 1-D flux for water and proton along the normal vector to the electrode surfaces, *x*, we simply have (Figure 1);

$$J_{H_2O} = -D_{H_2O}\left(\frac{\partial C_{H_2O}}{\partial x}\right) + \frac{\psi^{o}{}_{H_2O}\, j_{cell}}{F} \qquad (6)$$

To study the temporal variations we need to consider that the time variations of C_{H_2O} is the opposite of the water flux gradient ∇J_{H_2O} similarly to the derivation of diffusion second Fick´s law:

$$\frac{\partial C_{H_2O}}{\partial t} = -\frac{\partial J_{H_2O}}{\partial x} = -\frac{\partial}{\partial x}\left(-D_{H_2O}\left(\frac{\partial C_{H_2O}}{\partial x}\right)\right) - \frac{\partial}{\partial x}\left(\frac{\psi^{o}{}_{H_2O}\, j_{cell}}{F}\right) \qquad (7)$$

To avoid complexities in mathematics we will not take into account the membrane microscopic change before and after water entrance only a homogeneous medium. Also, diffusivity and water transference number are taken as constants, that is, no change in elastic forces or conformations of hydrophilic ionic terminals.

According to [14] and [27, 28] it is possible to evaluate the electroosmotic drag as a Series Expansion, each term with distinct power pounding in the local concentration $\psi^{o}{}_{H_2O} = \sum_i \psi_{H_2O}{}^{i} C_{H_2O}{}^{i}(x)$. We are going to consider only a first linear term to solve the differential equation (7), *i.e.* $\psi^{o}{}_{H_2O} = \psi_{H_2O} C_{H_2O}(x)$.

After substitution we have:

$$\frac{\partial C_{H_2O}}{\partial t} = D_{H_2O}\left(\frac{\partial^2 C_{H_2O}}{\partial x^2}\right) - \frac{\psi_{H_2O}\, j_{cell}}{F}\left(\frac{\partial C_{H_2O}}{\partial x}\right) \tag{8}$$

In terms of Electrochemistry, the operation of the fuel cell under steady state conditions implies a galvanostatic or step to step gavanodynamic type of measurement. Thus, $\mathbf{j_{cell}}$ will be constant and the second term pre-multiplying the single derivation of concentration with velocity units will be taken as $\mathbf{v_{H2O}}$**,** indicating a fully developed flow under constant current densities**.**

$$DC_{H_2O} \equiv \frac{\partial C_{H_2O}}{\partial t} + v_{H_2O}(x,t)\left(\frac{\partial C_{H_2O}}{\partial x}\right) = D_{H_2O}\left(\frac{\partial^2 C_{H_2O}}{\partial x^2}\right) \tag{9}$$

With $v_{H_2O}(x,t) = \frac{\psi_{H_2O}\, j_{cell}}{F} = \frac{\psi^{o}{}_{H_2O}\, j_{cell}}{F C_{H_2O}(x)}$ (10)

Then,

$$DC_{H_2O} \equiv \frac{\partial C_{H_2O}}{\partial t} + \frac{\psi^{o}{}_{H_2O}\, j_{cell}}{C_{H_2O}(x) F}\left(\frac{\partial C_{H_2O}}{\partial x}\right) = D_{H_2O}\left(\frac{\partial^2 C_{H_2O}}{\partial x^2}\right) \tag{11}$$

1.- Under steady state regimes reduces to the equation;

$$\left(\frac{\partial^2 C_{H_2O}}{\partial x^2}\right) - \frac{\psi^{o}_{H_2O}\, j_{cell}}{D_{H_2O} F}\left(\frac{\partial C_{H_2O}}{\partial x}\right) = 0 \qquad (12)$$

This differential second order ordinary equation is easily solved since it is a homogeneous linear equation with constants coefficients. However we have to take care on the definition of the initial and contour conditions.

a)When there is no water at the anode and full maximum at the cathode C^o;

$$C_{H_2O}(x = 0) = 0 \qquad C_{H_2O}(x \to \infty) = C^{o} \qquad (13, 14)$$

The solution is;

$$C_{H_2O}(x) = C^{o}\left(1 - e^{\frac{-\psi^{o}_{H_2O}\, j_{cell}}{D_{H_2O} F} x}\right) \qquad (15)$$

b)When the initial condition implies a starting maximum water concentration, C^o:

$$C_{H_2O}(x = 0) = C^{o} \qquad (16)$$

The solution is now:

$$C_{H_2O}(x) = C^{o}\left(e^{\frac{-\psi^{o}_{H_2O}\, j_{cell}}{D_{H_2O} F} x}\right) \qquad (17)$$

2.- In the case of non-steady state conditions the equation to solve is;

$$\left(\frac{\partial C_{H_2O}}{\partial t}\right) + \frac{\psi^{o}_{H_2O}\, j_{cell}}{D_{H_2O} F}\left(\frac{\partial C_{H_2O}}{\partial x}\right) = D_{H_2O}\left(\frac{\partial^2 C_{H_2O}}{\partial x^2}\right) \qquad (8)$$

The resolution of this partial differential equation can be accomplished by Laplace Transform considering a new function of convolution. A similar method of resolution was accomplished in [14, 29]. The above equation will be solved using the initial and contour conditions:

1.- $C_{H_2O}(x, t = 0) = C^{o} x \neq 0 \quad t > 0$ (18a)

2.- $C_{H_2O}(x \to \infty, t) = cteC^{o} \quad t \geq 0$ (18b)

3.- $j_{H_2O}\Big|_{x=0} = v_{H_2O,x=0} C_{H_2O} - D_{H_2O}\left(\frac{\partial C_{H_2O}}{\partial x}\right)_{x=0} \qquad x = 0, t > 0$ (18c)

The found analytical solution at *x*=0 is:

$$c(x=0,t) = \left(1 + \frac{v_{H_2O}^2 t}{2D_{H_2O}}\right) erfc\left(\sqrt{\frac{v_{H_2O}^2 t}{4D_{H_2O}}}\right) - 2\sqrt{\frac{v_{H_2O}^2 t}{4\pi D_{H_2O}}} \exp\left(-\frac{v_{H_2O}^2 t}{4D_{H_2O}}\right) \quad (19)$$

This complex expression deserves analysis only at the nearby of the anodic side of the membrane where the hydration starts to operate. Typical values are; v_{H2O} =10^{-7} cm/s, t < 100 s, D_{H2O} = 2 10^{-5} cm^2/s, yielding $T=tv^2_{H2O,x}/4D_{H2O}$ ca. 10^{-4}. Thus, the approximation that we have taken will hold for practical devices, so the T->0 approach is used here. This function at x->0 is reduced to a simple equation by Power Series that yields for the 80 % of hydration;

$$C_{H_2O}(x, t \to 0) \cong 0.8C^{o}\left(1 - \sqrt{\frac{4v_{H_2O}^2 t}{\pi D_{H_2O}}}\right) \approx 0.8 - 1.8t^{1/2} \quad (20)$$

Materials and Methods.-

A single PEMFC was used of 200 cm^2 geometric area, with a MEA 10 cm x 20 cm geometric area and 183 microns thickness. A 0.4 mg cm^{-2} platinum loads on anode and 0.4-0.6 mg cm^{-2} on the cathode were employed as catalyst layers supported on Vulcan XC. The preparation of the MEA was detailed in another paper [30] with typical materials. The same configuration for the anode and cathode channels have been used, the patterns and sizes of the configurations investigated were those accordingly to preparation.

Bipolar Plates layout were cross-flow, with horizontal channels in the anode and vertical channels in the cathode, with different depths, widths and thicknesses as detailed below. The material used for the bipolar plate was high quality graphite from *Fuel Cell Store*. Gas Diffusion Layers from the same enterprise were used containing 5% of teflon and a micro porous layer to enhance the performance of the diffusion layer - catalyst layer interface. Different samples of Nafion 117 from Du Pont® were used to find the proper cleaning method detailed in [30].

Finally, we found repetitive and precise results for the isopiestic method using the following methodology. The membranes were firstly boiled in 3 % hydrogen peroxide for 30 min and then with concentrated HNO_3 for another 30 min. Then, they were boiled in water for 1 hr. at 80^{o}C, followed by immersion in 0.10 M HCl (analytical grade from Merck) for 24 hrs. and repeatedly rinsed in Millipore MilliQ^{+} water.

Since the surface area of each side of the MEA device has to be taken into account for current density calculations, a control of the real area was accomplished using an adsorption *stripping* experiment [31]. The selected model molecule for this purpose was carbon monoxide (99.997 %, < 2ppm C_xH_y from Linde Group). Adsorption experiments were conducted after bubbling through a deoxygenated 0.50 M sulfuric acid as supporting electrolyte until saturation without the presence of either the auxiliary (large platinum foil) or reference (capillary hydrogen platinum ensemble) electrodes to avoid contaminations. The oxidative voltammetric profile of the residues (anodic *stripping* experiments) were recorded for an admission potential of 0.05 V held for 2 min at a 10 mVs^{-1} sweep rate. The excess of dissolved carbon monoxide was removed with continuous argon (N50 from Air Liquide) bubbling and simultaneously exchanging with the supporting electrolyte keeping the potential at 0.05 V during all

the experiment. The active surface area of anodic and cathodic sides of the MEA were determined by the charge involved in the carbon monoxide anodic stripping profile in a cyclic voltammetry from 0.60 to 1.50 V assuming 420 μC cm^{-2} as total saturation charge density after the subtraction of the double layer charging contribution [31].

The 200 cm^2 PEM fuel cell adopted in the experimental measurements was home-made and developed in-house using a compact design. The MEA (Nafion 117) was prepared using a temperature-controlled hydraulic press. The humidified oxygen and hydrogen streams (up to 99.99 % purity of Linde Group) were thermostatised before the entrance in the fuel cell, which operates from 20 to 68^{o}C and occasionally at 80 to 90^{o}C. The polarization (power) curve of the PEMFC was obtained using a PGZ Potentiostat-galvanostat-impedance analyser from Radiometer Copenhagen (Software Voltalab 4 for the 32 System). The galvanodynamic program involves the application of increasing current steps, from 0.1 to 1.0 μA (depending on the curve region) for at least 3 min to reach stationary cell potentials in the range of the open circuit value (ca. 0.98 V for full hydration) and the lowest possible, that is ca. 0.1 V. At each current point, the stoichiometry of gases was calculated using Faradaic law and used to set the mass flow controllers.

The galvanostatic curves were also used to calculate the water content, λ, since it allows the application of the mass conservation formulae for λ after the substraction of a certain charge from the PEMFC. This charge is strongly dependent on λ in the MEA and it is the right way to study the steady state performance of the PEMFC.

The potential and power *vs*. current density curves were obtained from a clasically adapted experimental setup [32] as that shown in Figure 2. The most

important feature is the continuous humidification of gases at the entrance of the fuel cell and thermostatised conditions of work.

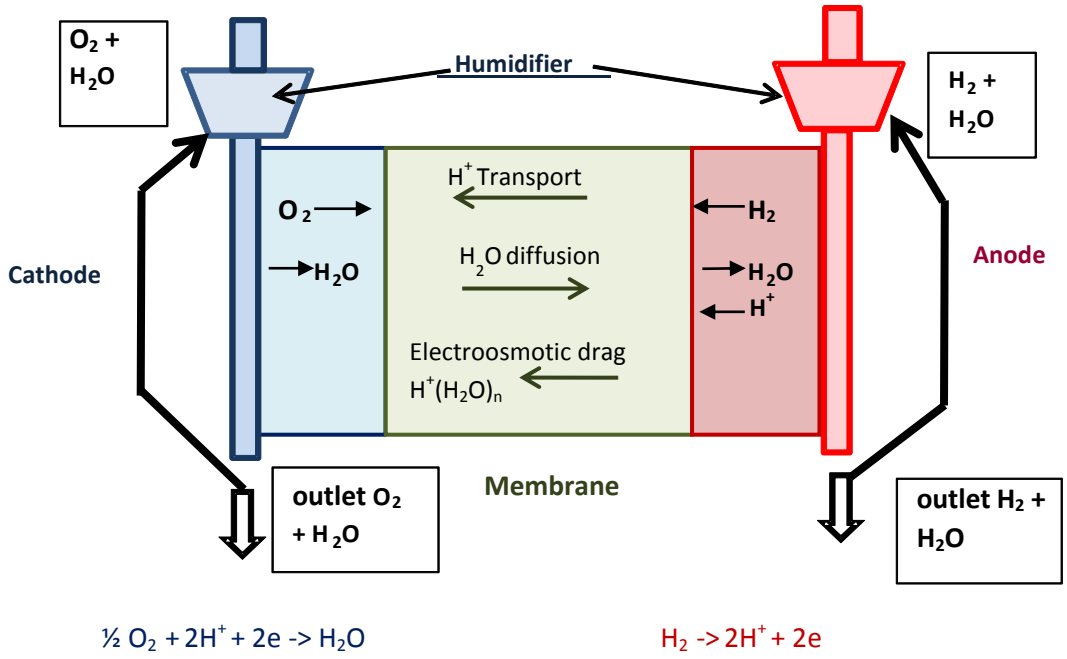

Figure 2.- Scheme of the PEMFC model with the entrance and recirculation of water on both sides.

For medium-time measurements (larger than 10 min), the galvanostatic determined λ in the membrane was checked by weighing the samples before and after drying. The sample was dried in vacuum at room temperature for 1 day and then at 110°C for another day. After cooling them down, they were weighed again and the water content calculated. This parameter is usually defined as the number of moles of water per mole of ion exchange site, $\lambda = H_2O/SO_3^-$, was:

$$\lambda = \frac{PM\ (m_1 - m_2)}{18.02\ m_1} \qquad (21)$$

Being *PM* the molar weight of the membrane and m_i the membrane weights before and after drying under vacuum.

Results.-

Water concentration profiles. Comparison between experimental and theoretical predicted values.

Figure 3 shows the dimensionless water concentration profile at the cathodic side of the MEA theoretical predicted from equation (19) plotted as a function of time varying distinct parameters. The experimental values (open squares) were also determined using the PEM ensemble described in the Experimental Section.

Panel (A) shows the effect on temperature for the normalised concentration of water. It is clear that the increase in the temperature produces a dehydration of the membrane faster than expected at 0.20 A cm^{-2}. Thus, the soft linear decline of catholyte water concentration at 313 K changes abruptly to a quasi-reciprocal square power decreases for 40 K higher measurements.

On the other hand, panel (B) depicts the effect of the increase in the current density at 293 K. A 1 order higher current from 0.05 to 0.5 A cm^{-2} produces a clear diminution of the water concentration due to a faster water consumption during the reaction.

The third plot in panel (C) exhibits the concentration change produced by the increase in the humidified hydrogen flow velocity (assumed as constant in the whole cell) in 1 order of magnitude. This growth produces a diminution in the concentration profile since, under the present experimental condition; the reactant is rapidly converted at the surface. When the current density or temperature (distinct to 293 K) is not optimized the behaviour can change to the opposite since the reactant gas could not be able to react at the electrode at a sufficient rate. Talking in linear velocities

terms, values larger than 10^{-6} cm s^{-1} do not produce any change in local water concentrations since hydrogen passes by without converting electrochemically in the cell. In this linear velocity, there is a dual control of volumetric flow rate, ***dV/dt*** and the exposed diffusion area, ***a***, expressed as its ratio.

$$v_{H_2O}(x=0) = \frac{\psi^{o}_{H_2O}\, j_{cell}}{C_{H_2O}(x=0)F} = \frac{dV}{dt} \Big/ area \qquad (22)$$

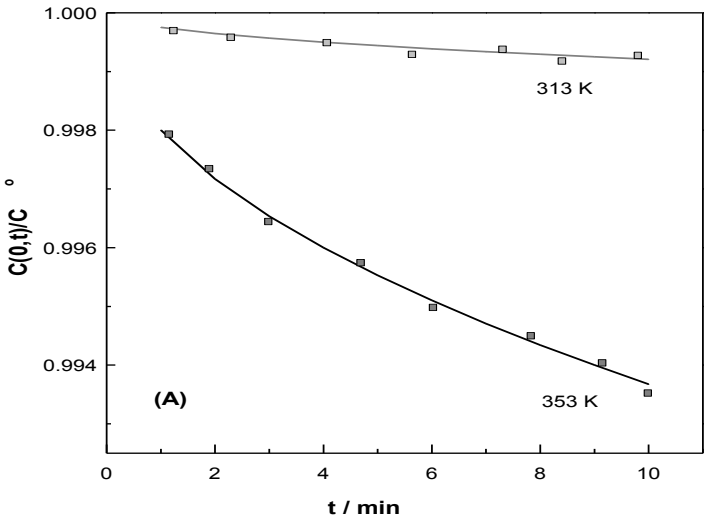

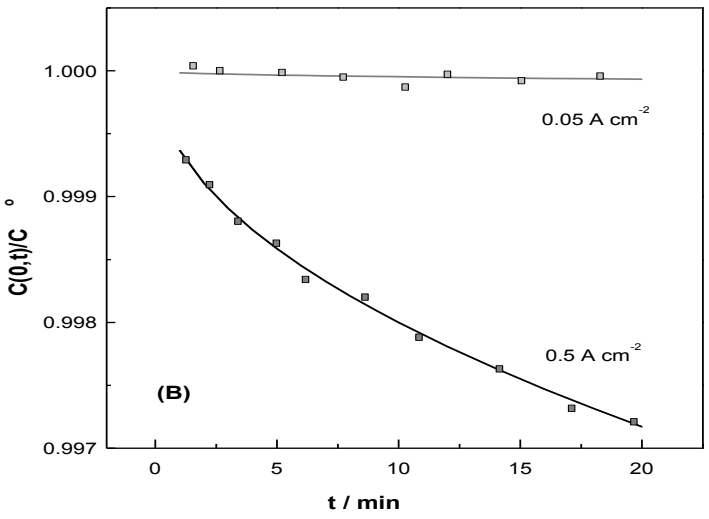

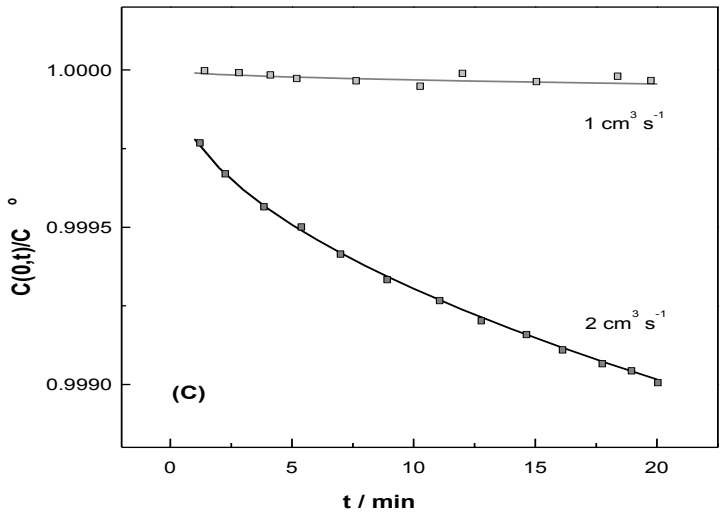

Figure 3.- Dimensionless concentration profile of water at the surface of the MEA (black and grey full lines), cathode side, as a function of time for: (A) different operation temperatures 313 (gray lines) and 353 K (black lines); (B) current densities 0.05 (gray lines) and 0.5 A cm^{-2} (black lines); (C) volumetric flow velocities defined from 1 (gray lines) and 2 cm^3 s^{-1} (black lines) volumetric flow rates. Experimental points are depicted as open squares (with experimental details explained in the Experimental Section).

The first two effects can be minimized using permanent water recirculation on the PEMFC under the same conditions.

Determination of the real surface area at the catalyst layer.

The following voltammetric plots show the carbon monoxide anodic *stripping* experiments for the anodic and cathodic sides, both with 0.4 mg cm^{-2} platinum loads, of the Nafion 117 MEA before starting the polarization curves. The most important

thing is that for a full water unity content, there is only an increase of 15 % of the surface cathodic area, while 5 % at the anodic side (determined using the same method) after the subsequent polarization curves of operating PEMFC. Due to the large surface roughness it was not possible to eliminate all adsorbed carbon monoxide by a single anodic sweep up to 1.25 V. However, it allows us to check for the different voltammetric peaks in a low carbon monoxide coverage range to envisage adsorbate configurations. The anodic side of the MEA exhibits mostly single adsorbed carbon monoxide species (0.73 V), whereas the cathodic side both single and bridge adsorbed species (0.75 and 0.80 V). Thus, at least 2 potential scans were needed (Figure 4) and the total anodic charge under the voltammetric profile for the carbon monoxide oxidation was taken as the addition of both potential sweep areas. The calculation of the anodic surface area was 16700 cm^2, while for the cathodic side was 17200 cm^2. Thus, there is no important difference between both areas and it is not necessary to correct current values before the PEMFC operation. However, the variance between the 2 areas gets wider for operation times larger than 10 min and then it will need some attention.

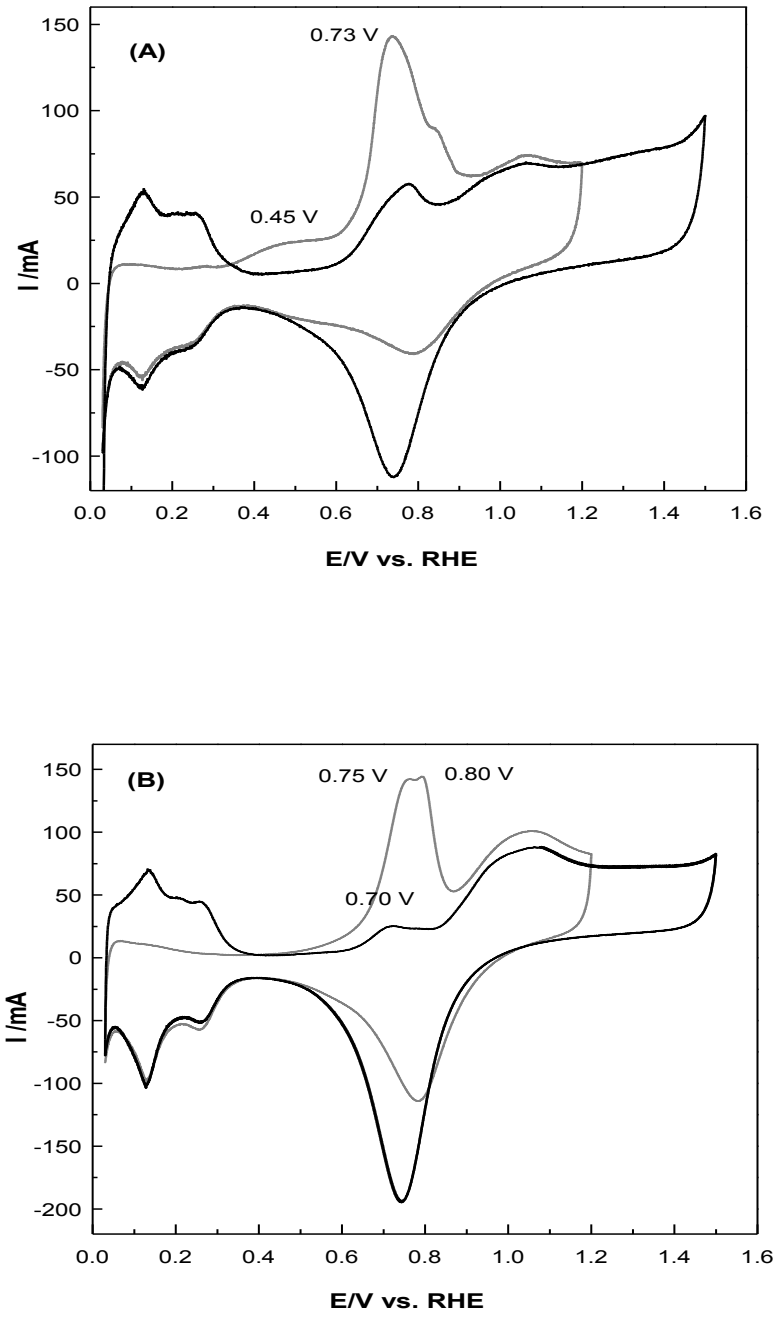

Figure 4.- Adsorbed carbon monoxide anodic *stripping* profiles run at 10 mV s^{-1} of adsorbed carbon monoxide formed at 0.05 V for 2 min as explained in the text. **(A)** anodic and **(B)** cathodic sides of the 117 Nafion MEA device. Platinum anodic and

cathodic loads are 0.4 mg cm^{-2}. The characteristic anodic *stripping* peaks are indicated in the figure.

Calculation of the electroosmotic drag coefficient.

For the determination of the electroosmotic drag coefficient, $\psi^{o}_{H_2O}$, a modified *isopiestic method* in an electrochemical cell was employed as detailed below. The measurements of the reversible zero current electrode potential, **E** and water activity was modified from those of the literature [32, 33]. The diagram of the 4 electrode thermostatic cell is this below:

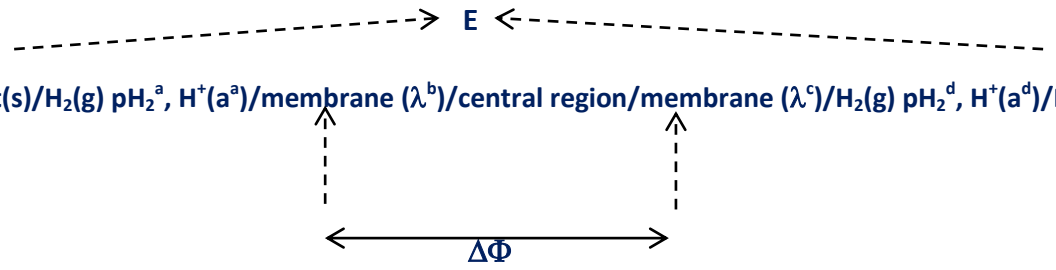

The measurements were conducted from the relative change in the water vapour pressure between 2 identical hydrogen platinum electrodes as **E**. As a matter of control the liquid junction potential difference, $\Delta\Phi$ in the central region, it was also measured using 2 identical reference electrodes with the same electrode potentials (previously short-cut for 2 months to achieve that condition, *Pinkhoff method*).

Different values of $\psi^{o}_{H_2O}$ were reported in the literature [8, 34] with varying conditions of moistening or hydrations, type and nature of membranes, pre-treatment

methods, determination techniques, etc. The values changes from 0.9 to 3.16 at extreme conditions of current densities (5 A cm^{-2}), temperatures ($60^{o}C$) and water contents (λ ca. 22).

In this work we have assayed 2 distinct temperatures, 313 and 353 K, for $\lambda < 5$ from which the following *E vs. log(P/P$_{sat}$)* plots were constructed according to the isopiestic method (Figure 5). The found values of $\psi^{o}_{H_2O}$ were 2.33 and 2.30 for 313 and 353 K, respectively, showing constancy with temperature. However, when working above 363 K, $\psi^{o}_{H_2O}$ rises to 3.2. At this temperature there are also problems of heat loss that produces some water evaporation, even when a thermostatted system was used. It seems that some non-compensated irreversible heat is produced, so no further experiments were conducted for higher temperatures. On the other hand, for increasing values of λ up to 20 there is a linear rise from $\psi^{o}_{H_2O}$ =2.3 up to 3.3 at 313 K.

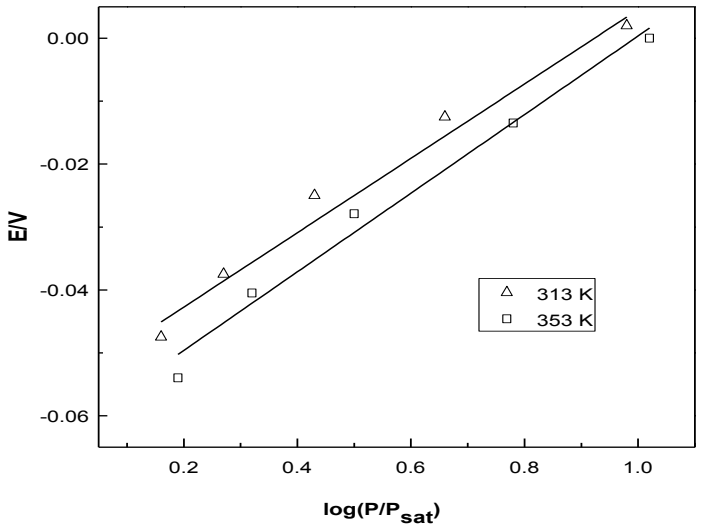

Figure 5.- Determination of water electroosmotic drag coefficient $\psi^{o}_{H_2O}$ in treated Nafion 117 membrane using the isopiestic method at 313 (open up triangles) and 353

K (open squares) with an electric potential, **E**, *vs.* logarithmic water vapour pressure ratio, **log(P/P$_{sat}$).**

For the calculation of the water concentration profile, $C_{H_2O}(x,t)$ we use the following parameters;

$$C_{H_2O}(x,t) = aP_{H_2O}{}^{g}\lambda C_{SO_3^-} = 1.62\,(0.001836\quad)P_{H_2O}{}^{g}\lambda \qquad (23)$$

Where $P_{H_2O}{}^{g}$ is the partial pressure of water vapour in the gas phase and $C_{SO_3^-}$ is the sulfonic group concentration $\rho_{drymemb} / PM_{memb} = 2.02/1100 = 0.0018\ \overline{36}$ and **a** is the membrane expansion volumetric factor $a = V_{dry}/V_{wet} = 1.62$.

Polarization curves for distinct water contents.

As explained above, the PEMFC polarization curve was performed using the galvanodynamic methodology since a constant charge applied to the FC is better to control and calculate the water content during the measurement. After applying a step to step current, the steady state potential of the cell was reached after ca. 3 min, but extends to 5 min near the limiting current density.

The performance of the PEMFC with 117 Nafion of different hydration ratios is exhibited in Figure 6 as potential and power density plots as a function of the current density. The plots are constructed at 338 K for 0.4 and 0.8 (40 and 80 %) relative content of water for 180 microns of thickness. There is an important affectation of the open circuit potential and the limiting current density decreases only a little indicating that the membrane is moistening during operation. The slope of the curve is the

internal resistance of the cell and it clearly changes from 0.59 Ω cm^{-2} for 0.8 and 0.24 Ω cm^{-2} for a 0.4 water relative content. The slope is linear only when humidified entrance gases are used, thus, it seems that for increasing volumetric flow rates water is permanently hydrating the MEA device. However, this has to be taken with care to avoid flooding. There is another interesting point and it is the difficulty to reach the limiting current for low water contents, obeying to the partial dehydration the MEA during operation. However, it all depends on the current values and gas entrance flow rates. Moreover, the open circuit potential is also affected by the lack of water, only 0.38 V, a fact *a priori* not expected.

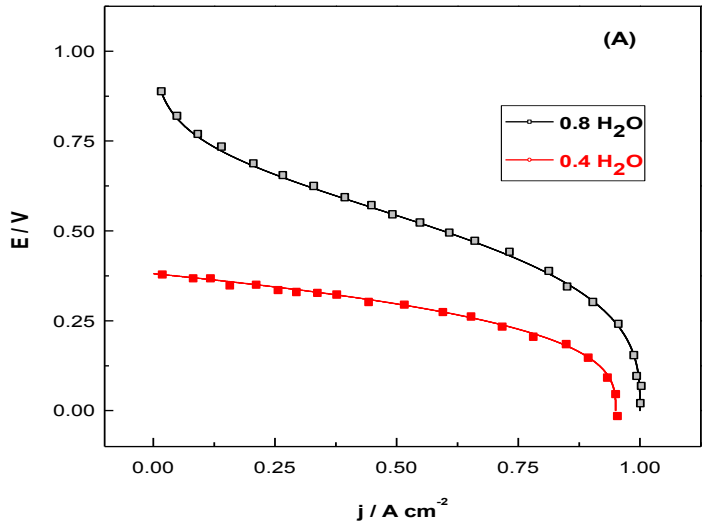

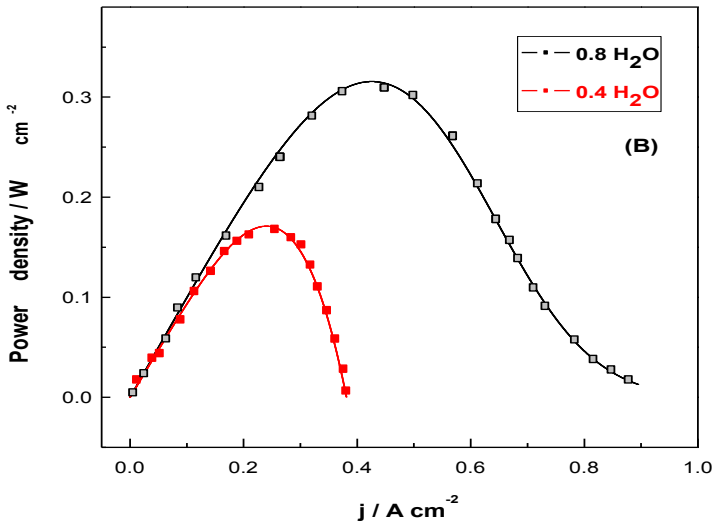

Figure 6.- Polarization galvanodynamic curve, potential vs. current density **(A)** and power density vs. current density **(B)** curves at 338 K for 0.4 (red bold squares) and 0.8 (black open squares) water amounts with anode and cathode humidifiers but no recycling. Inlet anodic and cathodic humidified gases flow rates 1.8 and 1.6 ml min^{-1}, respectively. Nafion 117 Membrane thickness 180 microns and anode/cathode catalyst layer thicknesses ca. 0.5 microns.

The main aspect in the power density curve for comparison is the possibility of control the mass transport components near the limiting current density. There is a strong decrease in the power maximum value at the 0.4 low water relative content; 0.31 W cm^{-2} for 0.8 and 0.17 W cm^{-2} for 0.4 water relative amounts.

The decrease in the membrane water content was then solved by continuous water recycling; even so, high current densities are also observed for 0.4 water relative content. Thus, the slope of the polarization curve, that is, the internal resistance is mainly affected by the membrane resistivity which is directly affected by inconstancies in the presence of water along the membrane.

On the water dependent membrane resistivity.

Ohmic overpotential is controlled by electric and mechanical characteristics of every material that constitutes PEMFC: as the bipolar plates, gas diffusion layers, catalyst layers, current collectors and the MEA. They are all proportional to each thickness and reciprocal to their electrical conductivity. The contact resistance between gas diffusers and the bipolar plate has been gathered and well defined in the ohmic overpotential to the performance of the PEMFC [33].

The total proton conduction resistance R_M of the membrane and anode catalyst layer is calculated using Eq. (24) for no saturation of cathode outlet water vapour, being S the real surface area of the interface previously determined by carbon monoxide anodic stripping voltammetry and σ_M the membrane conductivity function of water content, λ. This area can be restricted also to the overflowing of water as explained below.

$$R_M = \int_0^d \frac{dx}{S\,\sigma_M} \tag{24}$$

with x the water molar fraction estimated by the Stefan-Maxwell equation.

From the latter interdiffusion expression we can obtain the gradient of the water molar fraction with the coordinate, **z**, along the membrane in the anode;

$$\frac{dx^{a}_{H_2O}}{dz} = \frac{RT}{F}\, j_{cell}\, \frac{[\,x^{a}_{H_2O}(1+\Theta)-\Theta\,]}{P^{a} D_{H_2O,H}} \tag{25}$$

Being Θ the ratio between the water flux in the membrane and that produced at the cathode, j_{cell} is the current density along the fuel cell, P^a the water pressure at the anode and $D_{H2O,H}$ the binary diffusivity of water caused by proton migration.

And after integration between $x^{a}_{H_2O} = x_1$ at z=0 and $x^{a}_{H_2O} = x_2$ at z=d;

$$x_2 = \frac{\Theta}{\Theta + 1} + \left(x_1 - \frac{\Theta}{\Theta + 1} \right) \exp \left(\frac{RT}{F} \frac{dj_{cell}}{P^{a} D_{H_2O,H}} \right) \qquad (26)$$

Thus, using the Nernst-Einstein relationship between $D_{H2O,H}$ and its mobility we can envisage an expression for the conductivity, σ_M as a function of λ (linear relationship including temperature) as shown before [34].

$\sigma_M = (a\lambda + b) \exp \left(\frac{c}{T_1} - \frac{c}{T_2} \right)$ for $\lambda > 1$ being ***a, b*** and ***c*** experimental parameters.

(27)

According to the referred connection between water activity (below unity) and λ water content the employed by Springer *et al.* [13] at 303 K was also used here;

$\lambda = 0.043 + 17.81\, a - 39.85\, a^2 + 36.0\, a^3$ and $a = xP_{dif.} / P_{sat}$ (28 a, b)

According to our experimental results we obtained, a= 0.0052, b= -0.0031, c= 1250. We compared these figures with the $\mathbf{R_M}$ values obtained from the polarization curves. The results were similar to those obtained by Hong *et al.* [35] at 353 K.

On the water recycling of the PEMFC.

The idea was to minimise the water excess or defect in the PEMFC, so the water anolyte and catholyte mass balances at a certain time, $n_{H2O,a}$ and $n_{H2O,cat}$ have to be measured as the derivation with time of these magnitudes. Both consider the flux variation in the membrane per unit of effective area, being the difference of the molar fluxes from anode to cathode by electroosmotic drag and that of the diffusion in the opposite direction due to the concentration gradient;

$$J_{H_2O}^{mem} = \frac{dn_{H_2O}^{mem}}{Sdt} = \frac{dn_{H_2O}^{drag}}{Sdt} - \frac{dn_{H_2O}^{dif}}{Sdt} \tag{29}$$

As we have shown above the fluxes depend on the current developed by the cell, $j_{cell}=I_{cell}/S$ per effective area S, and water content in the membrane, λ.

$$S_{an} J_{H_2O}^{an} = \frac{dn_{H_2O,an}^{in}}{dt} - \frac{dn_{H_2O,an}^{out}}{dt} - \frac{dn_{H_2O}^{mem}}{dt} \tag{30a}$$

$$S_{cat} J_{H_2O}^{cat} = \frac{dn_{H_2O,cat}^{in}}{dt} - \frac{dn_{H_2O,cat}^{out}}{dt} - \frac{dn_{H_2O}^{mem}}{dt} + \frac{dn_{H_2O}^{gen}}{dt} \tag{30b}$$

With; $\frac{dn_{H_2O}^{gen}}{dt} = S_{cat}\, j_{cell} / 2F$ (30c)

We need to develop new formulae to envisage experimental parameters defining the minimum loss of water with recycling. Thus, the inlet molar water flow is;

$$\frac{dn_{H_2O,an}^{in}}{dt} = k_{an}^{in} x_{H_2O,vap}^{in,an} (p_{an}^{in} - p_{an}) \tag{31}$$

Being k_{an}^{in} the adjustable parameter, p_{an}^{in} the inlet pressure at the anode and p_{an} the pressure of water in the anode electrode and $x_{H_2O,vap}^{a}$ the water vapour molar fraction in the inlet flow.

With $p_{an} = p_{H_2O,vap,an} + p_{H_2O,gas,an}$ (32)

Being the pressures at the right hand side the partial magnitudes of the vapour and dry gas, respectively, in the electrode.

And $x_{H_2O,vap}^{in,an} = \frac{h_{H_2O}^{in,an} p_{H_2O,an}^{sat}}{h_{H_2O}^{in,an} p_{H_2O,an}^{sat} + (p_{an}^{in} - h_{H_2O}^{in,an} p_{H_2O,an}^{sat}) 2/18}$ (33)

The magnitudes presented as $h_{H_2O}^{in,an}$ is the relative humidity of inlet gases, molar weight 2 for dry molecular hydrogen and 18 for water vapour, at a constant inlet temperature without the presence of liquid water.

On the other hand, the dry gas and water vapour can obey the ideal gas law at the inlet temperature at the anode;

$$p_{gas,an} = RT^{in,an} \frac{n_{H_2,an}^{in}}{V^{an}} \tag{34a}$$

$$p_{H_2O,vap,an} = RT^{in,an} \frac{n_{H_2O,an}^{in}}{V^{an}} \tag{34b}$$

Besides, the water leaving an electrode is separated into liquid and vapour phases due to differences in their flow properties. Thus, the outlet molar water flows are;

$$\frac{dn_{H_2O,an}^{out}}{dt} = \frac{dn_{H_2O,vap,an}^{out}}{dt} + \frac{dn_{H_2O,liq,an}^{out}}{dt} \tag{35}$$

$$\frac{dn_{H_2O,vap,an}^{out}}{dt} = k_{an}^{out} x_{H_2O,vap}^{out,an} (p_{an} - p_{an}^{out}) \tag{36}$$

With similar meaning as the inlet parameters.

The new instance is the consideration of $\frac{dn_{H_2O,liq,an}^{out}}{dt}$ the liquid water drained out from the electrode, that has to be de difference between the accumulated molar liquid water and the pressure drop across the electrode;

$$\frac{dn_{H_2O,liq,an}^{out}}{dt} = g_{H_2O,liq,an}^{out} (p_{an} - p_{an}^{out}) \tag{37}$$

Being the magnitude $g_{H_2O,liq,an}^{out}$ the characteristic geometric parameter of the anode (bipolar plate), material and the amount of liquid water evaluated as the difference between the total water number of moles and that of vapour water.

Similar dynamics occur in the cathodic side of the fuel cell.

In those equations, the electrode inlet conditions, that is, inlet pressures p_{an}^{in} and p_{cat}^{in} and inlet humidities $h_{H_2O}^{in,an}$ and $h_{H_2O}^{in,cat}$ modify the flows into the two sides of the MEA. Meanwhile, the flows out of the electrodes are affected by the electrode exit conditions p_{an}^{out} and p_{cat}^{out} . However, the adjustable parameters $k_{electrode}^{in}$ and $g_{H_2O,liq,electrode}^{out}$ for anode and cathode allows the minimization of water losses and then, an optimal recycling can be accomplished.

This process can be conducted by iteration, however, a typical set of physical parameters have been used. The first ones are the anodic and cathodic inlet pressures, 0.3 and 0.6 MPa, respectively with relative humidities of 80 %. With these data and physicochemical parameters, such as, dry membrane density, molecular weights, the molar fraction by water at the anode and cathode render distinct values for $k_{electrode}^{in}$; 0.32 and 0.11 g s^{-1} Pa^{-1} for cathode and anode, respectively.

For the other parameter $g_{H_2O,liq,electrode}^{out}$ a flow design of 7 to 10 channels has been used and 2 depths, 0.60 mm to 0.25 mm, have been assayed. We have seen that as the depth decreases, the current density increases to ca. 12%, therefore we have employed the lowest as possible (0.25 mm). This is because the attenuation in the depth of the channel increases the convective flow, helping to the exclusion of excess liquid water, and thus avoiding flooding. A similar condition was taken into account for the channel width using from 2.5 to 1.25 mm, being the lower one, the best of performing.

On the other hand, as the oxygen volumetric flow rate increases from 1 to 2 cm^3 s^{-1}, the PEMFC performance enhanced due to the incoming of oxygen and therefore, it

increases the removal rate of water excess, at 293 K or below. At temperatures higher than 293 K the effect is the opposite, that is, the current density reduces to less than 15% when growing the oxygen volumetric flow rate to the double because the electrochemical reactions rate do not accompany the enhanced hydrodynamics.

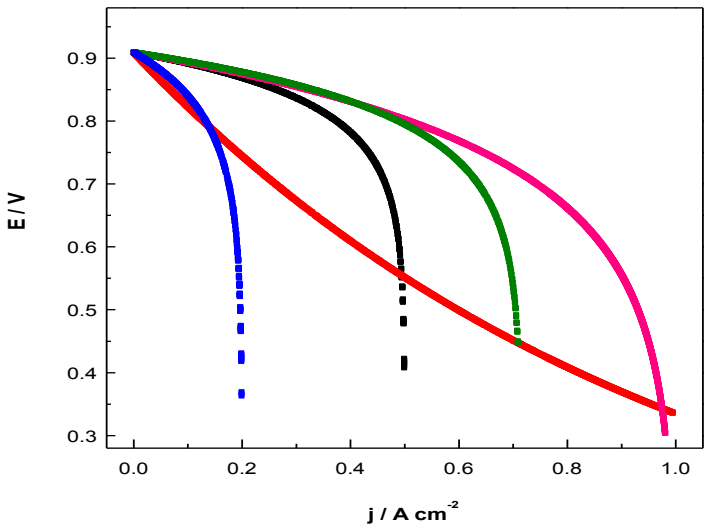

Figure 7.- Polarization galvanodynamic curves, potential vs. current density, recorded after 24 hour operation times for different water membrane conditions. The curve with a PEM cell of a 1 H_2O ratio content is depicted with green lines; without any humidification as red lines; with water permanent recycling (pink lines). Equivalent polarization curves were constructed with no water exit and plotted as black lines and in the situation of flooding conditions as blue lines. The experimental characteristics are those shown in Figure 6.

Polarization curves (Figure 7) for water saturation conditions at 353 K after 24 hrs. operation times are plotted as green lines. The pink lines show the same curve under water recycling conditions, denoting little changes in the membrane internal

resistance. Thus, it does not obey a different experimental behaviour, but a continuous drawn and entrance of water to the PEMFC. Red lines´s curve shows the comparative operation plot without humidification or recycling. Here it is clear a decrease in the performance with almost a constantly linear decay with current density, typical of an ohmic controlled process.

When the PEMFC works at low current densities with low relative humidity of inlet flows, the water vapour at cathode outlet is usually not saturated. Another indication is that the pressure difference between the inlet and outlet of cathode is small. Under full operating conditions, the net water generation to be drained is the addition of the water flux from anode to cathode and water formation by the electroreduction reaction. By the measurement of the anode characteristics, the precise estimation of the whole water flux coefficient contributes to the estimation of local water content at the cathode interface. The uniformity of component distribution along the flow channel can be guaranteed for a fuel cell of large surface area, the polarization curve is that shown in the Figure 7 as black lines.

However, it is usually more important to work at high current densities to deliver maintainable power and to cover the high surface area of the PEMFC. Under this condition the produced water in the cathode cannot be totally exhausted as water vapour and some liquid water arises in the downstream of the cathode channel. Consequently, the oxygen gas transport in the diffusion layer is banned from getting to reaction electrode sites since liquid water shield them. Thus, there is a small difference between inlet and the larger outlet stream and the fuel cell potential rapidly diminishes because of flooding, showing the polarization curve depicted as blue lines. The calculation of the internal resistance will exhibit larger values due to this factor.

The water flow into the inlet channels is also established by the temperatures of the external gas humidifiers and that of the cell. Water vapour is balanced under the saturation pressures by the defined humidifier temperatures in the inlet flow streams. These liquid condensations are moulded and transported with the gas flow stream if the cell temperature is less than the humidifier temperature. However, these droplets will evaporate again in the inlet flow channels if the operating condition of the humidified fluid develops below saturation. Entrained droplets become a transport mechanism for water under isothermal conditions. On the other hand, the flooding of the electrodes can occur when large excess of water is found, so in this sense a careful recycling was operating using energy thermal balances. Water vapour or liquid leaves the two inlet flow channels accordingly.

Conclusions.-

The out of regime water concentration profiles have been obtained analytically using mass transport equations, finding complex equations that are simplified at the surface of electrodes and small times of operation.

The electroosmotic drag coefficients have been determined using an electrochemical isopiestic procedure yielding values ca. 2 (for water contents less than 5) independent of temperature between 313 and 353 K, but increases to 3 for 363 K and water contents up to 20 at 313 K.

The real active surface area of the cathode and anode, ca. 0.4-0.6 mg cm^{-2} Pt loads, was determined before and after polarization curves using carbon monoxide anodic *stripping* method, being 16700 and 17200 cm^2 for the anodic and cathodic sides, respectively.

The effect and control of water content along the membrane of a PEMFC has been studied experimentally by galvanodynamic polarization curves employing water recycling method to keep constantly humid the membrane. Thus, we introduced 4 parameters; 2 of them for the humidified inlet gases and the rest for geometric flow patterns in the bipolar plates and diffusion layers. The results have been compared with distinct experimental situations of flooding, saturation, no recycling, etc.

Acknowledgements.-

C.F.Z. wishes to thank ANII, PEDECIBA, and CSIC (from Udelar) for the experimental support. C.F.Z. is a researcher at PEDECIBA and ANII.

References

[1] F. Barbir, PEM Fuel Cells, Elsevier Academic Press, Burlington, 2005.

[2] *Handbook of Fuel Cells: Fundamentals, Technology, Applications*, 4 Volume Set, 1st Ed., Wiley (2003) W. Vielstich , A. Lamm, H. A. Gasteiger (Editors) ASIN : 0471499269.

[3] P.L. Reid, U.S. Patent No. 4, 759 (1988) 882.

[4] T.V. Nguyen, R.E. White, J. Electrochem. Soc. 140 (1993) 2178–2186.

[5] C.Y. Chow, B.W.Wozniczka, U.S. Patent No. 5, 382 (1995) 478.

[6] Y. Chang, Y. Qin, Y. Yin, J. Zhang, X. Liab, Appl. Eenergy 230 (2018) 643-662.

[7] A. Zhamu, J. Guo, B. Z. Jang, US 7993791B2, United States (2005) Nanotek Instruments Group LLC.

[8] W. Dai, H. Wang, X.-Z. Yuan, J. J. Martin, D. Yang, J. Qiao, J. Ma, Int. J. Hydrogen Ener. 34 (2009) 9461-9478.

[9] T. A. Zawodzinski, C. Derouin, S. Radzinski, R. J. Sherman, V. T. Smith, T. E. Springer, J. Electrochem. Soc. 140 (1993) 1041–1047.

[10] D. R. Morris, X. Sun, J. Appl. Polym. Sci. 50 (1993) 1445–1452.

[11] D.M. Bemardi, J. Electrochem. Soc. 137 (1990) 3344.

[12] T.F. Fuller, J. Newman, J. Electrochem. Soc. 139 (1992) 1332–1337.

[13] T.E. Springer, T.A. Zawodzinski, S. Gottesfeld, J. Electrochem. Soc. 138 (1991) 2334-2342.

[14] T. Okada, G. Xie, Y. Tanabe, J. Electroanal. Chem. 413 (1996) 49-65.

[15] S. Park, I.-H. Oh, J. Power Sources 188 (2009) 498–501.

[16] P. Hong, L. Xu, J. Li, M. Ouyang, Int. J. Hydrogen Ener. 42 (2017) 18540-18550.

[17] B. S. Lee, H. Y. Park, I. Choi, M. K. Cho, H. J. Kim, S. J. Yoo, J. Power Sources 309 (2016**)** 127.

[18] A. Y. Karnik, A. G. Stefanopoulou, J. Sun, J. Power Sources 164 (2007) 590-605.

[19] M. Zhu, X. Xie, K. Wu, A. U-Hassan Najmi, K. Jiao, 10th International Conference on Applied Energy (ICAE2018), 22-25 August 2018, Hong Kong, China, Energy Procedia, 158 (2019) 1724–1729.

[20] J. A. Salva, A. Iranzo, F. Rosa, E. Tapia, Energy 101 (2016) 100-112.

[21] Analytical Modelling of Fuel Cells, A. A. Kulikovsky, Ed. 1st. Ed. Amsterdam, Elsevier Science (2010).

[22] A. P. Sasmito, E. Birgersson, A .S. Mujumdar, Heat Transf. Eng. 32 (2011) 151-167.

[23] L. Z. Zhang, W. Z. Yuan, Sci. Technol. Built Environ. 23 (2017) 60-71.

[24] Reduced Modelling of Planar Fuel Cells: Spatial Smoothing and Asymptotic Reduction, Z. He, H. Li, K. E. Birgersson, Switzerland, 1st. Ed. Springer (2017).

[25] D.M. Bernardi, M.W. Verbrugge, AIChE J. 37 (1991) 1151–1163.

[26] T.E. Springer, T.A. Zawodzinski, M.S. Wilson, S. Gottesfeld, J. Electrochem. Soc. 143 (1996) 587–599.

[27] Non-equilibrium thermodynamics and physical kinetics, H. Bikkin, I. I. Lyapilin, Berlin, Boston, De Gruyter, 2014.

[28] Non-equilibrium thermodynamics of heterogeneous systems, S. Kjelstrup, D. Bedeaux, Hackensack, N.J., 2008.

[29] T. Okada, S. Kjelstrup Ratkje, H. Hanche-Olsen, J. Membr. Sci. 66 (1992) 179-192.

[30] E. Teliz, V. Diaz, I. Pérez, M. Corengia, C. F. Zinola, Int. J. Hydrogen Ener. 37 (2012) 14761-14768.

[31] C. F. Zinola, J. Solid State Electrochem. 23 (2019) 883-901.

[32] T.E. Springer, T.A. Zawodzinski, S. Gottesfeld, J. Electrochem. Soc. 138 (1991) 2334–2342.

[33] T. A. Zawodzinski, J. Davey, J. Valerio, S. Gottesfeld, Electrochim. Acta 40 (1995) 297–302.

[34] M. H. Akbari, B. Rismanchi, Renew. Ener. 33 (2008) 1775-183.

[35] P. Hong, L. Xu, J. Li, M. Ouyang, Int. J. Hydrogen Ener. 42 (2017) 18540-18550.